Neck formation and deformation effects in a preformed cluster model of exotic cluster decays

Satish Kumar* and Raj K. Gupta
Physics Department, Panjab University, Chandigarh-160014, India
(Received 29 November 1995; revised manuscript received 21 August 1996)

Using the nuclear proximity approach and the two center nuclear shape parametrization, the interaction potential between two deformed and pole-to-pole oriented nuclei forming a necked configuration in the overlap region is calculated and its role is studied for the cluster decay half-lives. The barrier is found to move to a larger relative separation, with its proximity minimum lying in the neighborhood of the Q value of decay and its height and width reduced considerably. For cluster decay calculations in the preformed cluster model of Malik and Gupta, due to deformations and orientations of nuclei, the (empirical) preformation factor is found to get reduced considerably and agrees nicely with other model calculations known to be successful for their predictions of cluster decay half-lives. Comparison with the earlier case of nuclei treated as spheres suggests that the effects of both deformations and neck formation get compensated by choosing the position of cluster preformation and the inner classical turning point for penetrability calculations at the touching configuration of spherical nuclei. [S0556-2813(97)04612-2]

PACS number(s): 23.70.+j, 23.60.+e, 21.60.Gx

I. INTRODUCTION

The models of exotic cluster decays are broadly classified [1] as the preformed cluster models (PCM) and the unified fission models (UFM). They are mainly distinguished by the inclusion or noninclusion of the concept of cluster preformation probability P_0. The inclusion of P_0 in PCM refers to the nuclear structure effects present in the decaying nucleus, which are completely ignored in fission models. Thus, the decay constant λ (or the decay half-life time $T_{1/2}=\ln 2/\lambda$) in a PCM is given by

$$\lambda_{\mathrm{PCM}}=P_0\nu_0 P, \tag{1}$$

which in a UFM becomes simply

$$\lambda_{\mathrm{UFM}}=\nu_0 P. \tag{2}$$

Here, ν_0 and P are respectively the barrier assault frequency and the barrier penetration probability. The straightforward difference between Eqs. (1) and (2) allows us to associate (with UFM) an empirical P_0,

$$P_0^{\mathrm{emp}}=\frac{\lambda_{\mathrm{expt}}}{\lambda_{\mathrm{UFM}}}, \tag{3}$$

whose value is unrealistically large ($\sim$0.1 to 10) for most of the fission models [2–6], except for one calculation [7] where $P_0^{\mathrm{emp}}\sim 10^{-11}$–$10^{-23}$, depending on the size of emitted cluster (^{14}C to ^{28}Mg) taken to be deformed wherever applicable.

One important aspect that remains to be treated properly in *all* the above noted models of exotic cluster decays is the undetermined nature of the interior part of the interaction potential where the emitted cluster overlaps with the daughter nucleus ($R_0\leqslant R\leqslant R_t$; R_0 is the equivalent spherical radius of the parent nucleus and R_t is the touching configuration radius of the cluster and daughter nuclei). Choosing the $V(R_0)=Q$ value of decay, the potential $V(R_0\leqslant R\leqslant R_t)$ is either approximated as a polynomial [2–5] (second order, third order, or a simple power law) or avoided completely [8] by choosing the inner turning point $R_a=R_t$ in the WKB integral. In this later work [8], the cluster preformation probability is also calculated at $R=R_t$. Alternatively, the Dirac-δ, the Michigan-3 Yukawa (M3Y) or the Christensen and Winther (CW) interactions [6,7,9] are used, which are strongly attractive in the interior region such that the inner turning point R_a is defined at a point where $V(R_a)=Q$ value. Here $R_a>R_0$.

In this paper, we attempt to determine the interaction potential for the overlap region, i.e., the $V(R<R_t)$, using the nuclear proximity approach [10,11] for deformed and oriented nuclei, and study its influence on exotic cluster decay properties of nuclei via the PCM of Malik and Gupta [8]. The neck formation effects are also included. The model of Malik and Gupta, which is reasonably successful and is applied extensively [12–18], uses the nuclear proximity potential between spherical nuclei for $R\geqslant R_t$ and avoids using the potential in the overlap region $R\leqslant R_t$. Thus, the present work is an extension of the PCM of Malik and Gupta wherein the missing deformation effects of both the cluster and daughter nuclei are included and the role of neck formation in the overlap region is analyzed. The interesting result of this study is that the barrier is lowered as well as narrowed down significantly and is moved to a larger separation distance. In the overlap region, the potential energy minimum (due to nuclear proximity) is shifted down in the close vicinity of the Q value and at a value of $R_{\mathrm{min}}>R_0$. Thus, for cluster decay studies a situation similar to that mentioned above for the Dirac-δ, the M3Y, or CW interactions [6,7,9] arises here, too.

In the PCM of Malik and Gupta, for the nuclei treated as spheres, the preformation factor P_0 is calculated theoretically at the touching point radius ($R=R_a=R_t$). In the present work, both daughter and cluster nuclei are deformed and the

*Present address: Physics Department, DAV College, Amritsar, Punjab, India.

initial turning point R_a refers to an overlapping ($R_a<R_t$) necked configuration. Thus, in the PCM of Malik and Gupta, it is an almost formidable task to determine the deformations of A−1 nuclei at all possible fragmentations, required for the calculations of P_0. One has to invoke the two center shell model for calculating the fragmentation potential $V(\eta)$ which requires carrying out a three-dimensional minimization in the deformations β_{21}, β_{22} of two nuclei and their necking-in parameter ϵ [$V(\eta)$ is used in the calculations of P_0, see below], or else resort to some simplifications. One such simplified calculation has been attempted, which shall be published separately [19]. Only some results of this calculation are given here. As an alternative way, in this paper we calculate $P_0^{\rm emp}$ and compare it with other model calculations which are known to give the cluster decay half-lives in good comparison with experiments [7,28]. A good comparison between the two P_0's would mean the same result for the measured and calculated decay half-lives.

In Sec. II, we discuss the nuclear proximity potential $V_P(R)$ separately for two non-necked deformed and oriented nuclei ($R\geqslant R_t$) and the necked system ($R<R_t$) formed in exotic cluster decays. The resulting total interaction potential $V(R)$ ($=V_C+V_P$; V_C being the Coulomb potential between the deformed cluster and daughter nuclei) is given in Sec. III. The PCM of Malik and Gupta [8] is briefly sketched in Sec. IV and our results of the calculation are presented in Sec. V. Finally, a summary of our results is added at the end in Sec. VI. For the early very brief reports of this work, see Refs. [1] and [20].

II. NUCLEAR PROXIMITY POTENTIAL

A. Non-necked surfaces

The proximity potential between any two curved surfaces is given by the ''pocket formula'' [10]

$$V_P(R)=4\pi\overline{R}\gamma b\Phi(\xi), \tag{4}$$

with

$$\Phi(\xi)=\begin{cases} -\frac{1}{2}(\xi-2.54)^2-0.0852(\xi-2.54)^3, & \xi\leqslant 1.2511,\\ -3.437\ \exp(-\xi/0.75), & \xi\geqslant 1.2511.\end{cases} \tag{5}$$

Here $\xi=s_0/b$, the shortest distance s_0 between the surfaces in units of b. The surface energy coefficient $\gamma=0.9517\{1-1.7826[(N-Z)/A]^2\}$ MeV fm^{-2}, and the surface thickness $b[=(\pi/2\sqrt{3}\ln 9)t_{10-90}]\approx 1$ fm for $t_{10-90}=2.4$ fm, the thickness of the surface in which the density profile changes from 90% to 10%. The universal function $\Phi(\xi)$ is defined for the overlap region ($R<R_t$), the touching configuration ($R=R_t$), and the separated surfaces ($R>R_t$).

For spherical nuclei $s_0=R-(C_1+C_2)=R-C_t$ and $\overline{R}$, the mean curvature radius is defined as

$$\overline{R}=\frac{C_1C_2}{C_1+C_2}, \tag{6}$$

where C_i ($i=1,2$), the Süssman central radii, are related to the effective sharp radii R_i as

$$C_i=R_i\left(1-\frac{b^2}{R_i^2}\right), \tag{7}$$

with $R_i=1.28A_i^{1/3}-0.76+0.8A_i^{-1/3}$. C_t represents the touching configuration for Süssman central radii.

For deformed and oriented nuclei, we follow the method of Malhotra and Gupta [11] where, for the geometry of two axially symmetric nuclei lying in the same plane (see Fig. 1 in Ref. [11]),

$$s_0=\frac{R\ \sin(\theta_1-\alpha_1)-R_2(\alpha_2)\sin\ \sigma}{\sin\ \psi_1}=\frac{R\ \sin(\theta_2+\alpha_2)-R_1(\alpha_1)\sin\ \sigma}{\sin\ \psi_2}, \tag{8}$$

with $R_i(\alpha_i)=R_{0i}[1+\beta_{2i}P_2(\cos\ \alpha_i)]$, $i=1$, 2, and $R_{0i}=1.15A_i^{1/3}$. The $\beta_{2i}=a_i/b_i$ is the ratio between major and minor axes. The angles α_i, ψ_i, and σ are given in terms of the orientation angles θ_i as follows:

$$\theta_1-\theta_2+180=\psi_1+\psi_2+\alpha_1+\alpha_2, \tag{9a}$$

$$\tan\ \psi_i=-R_i'(\alpha_i)/R_i(\alpha_i), \tag{9b}$$

$$\sigma=180-\psi_1-\psi_2=\alpha_1+\alpha_2-\theta_1+\theta_2, \tag{9c}$$

where $R'(\alpha)$ is the derivative of $R(\alpha)$ with respect to α and $\partial s_0/\partial\alpha_1=0=\partial s_0/\partial\alpha_2$. The angles α_i are the angles between the radius and the symmetry axis for each nucleus and are determined from Eqs. (9) by the iterative procedure [11].

The mean curvature radius R for two deformed nuclei, lying in the same plane, can be obtained from the relation

$$\frac{1}{\overline{R^2}}=\frac{1}{R_{11}R_{12}}+\frac{1}{R_{21}R_{22}}+\frac{1}{R_{11}R_{22}}+\frac{1}{R_{21}R_{12}} \tag{10a}$$

with

$$R_{i1}=\left|\frac{\{R_i^2(\alpha_i)+[R_i'(\alpha_i)]^2\}^{3/2}}{R_i''(\alpha_i)R_i(\alpha_i)-2[R_i'(\alpha_i)]^2-R_i^2(\alpha_i)}\right|,$$

$$R_{i2}=\left|\frac{R_i(\alpha_i)\sin\ \alpha_i\{R_i^2(\alpha_i)+[R_i'(\alpha_i)]^2\}^{1/2}}{R_i'(\alpha_i)\cos\ \alpha_i-R_i(\alpha_i)\sin\ \alpha_i}\right|, \tag{10b}$$

where $i=1,2$.

B. Necked surfaces

For the overlapping configuration ($R<R_t$), the above method [Eq. (4)] becomes less and less accurate as the overlap increases. Therefore, Malhotra and Gupta [11] have considered a necked configuration formed by two equal nuclei. In the following, we extend their derivation to the case of unequal nuclei, suitable for the exotic cluster decay process studied here and the collisions between two nonidentical nuclei.

In an adiabatic decay (or collision), a two center nuclear shape with a minimum of energy will be formed [Fig. 1(a)] which can be characterized by major and minor axes a_i and b_i (related to deformations β_{2i}), respectively, and the neck ϵ.

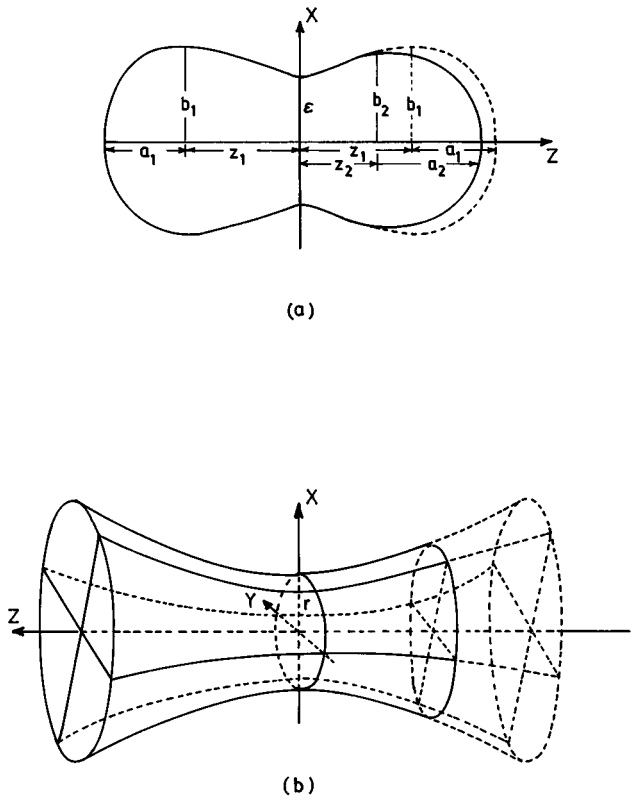

FIG. 1. (a) A characteristic two center nuclear shape formed during the decay of a nucleus into two equal (dashed lines) or unequal (solid lines) nuclei. (b) A schematic representation of a hyperboloid of revolution in one sheet formed due to equal (dashed lines) or unequal (solid lines) nuclei.

Thus, a single indented body in the form of a single hyperboloid of one sheet with a hyperboloidal crevice will be formed, as is shown in Fig. 1(b) (solid lines for unequal nuclei). For such a necked system, the proximity potential has the form [10,11]

$$V_P = \pi\gamma b^2 \frac{B^2}{C^2}\,\Phi_1(\xi=0), \tag{11}$$

where B and C are the semiaxes of the hyperboloid with C along the line of centers and $\Phi_1(\xi)$ is the first moment of the universal function (5) with $\Phi_1(\xi=0)=-2.0306$ (from Table I of Ref. [10]). In order to relate B and C to the parameters of two center nuclear shape in Fig. 1(a) (solid lines), we note that the equation of a hyperboloid of revolution in one sheet,

$$\frac{x^2}{C^2}+\frac{y^2}{C^2}-\frac{z^2}{B^2}=1, \tag{12}$$

gives

$$x^2+y^2=C^2\left(1+\frac{z^2}{B^2}\right)\equiv r^2, \tag{13}$$

the equation of a circle of radius r. From Fig. 1(a) (solid lines), we note that at $z=0$, $r=\epsilon$ and at $z=-z_1$, $r=b_1$; $z=z_2$, $r=b_2$, such that from (13) we get

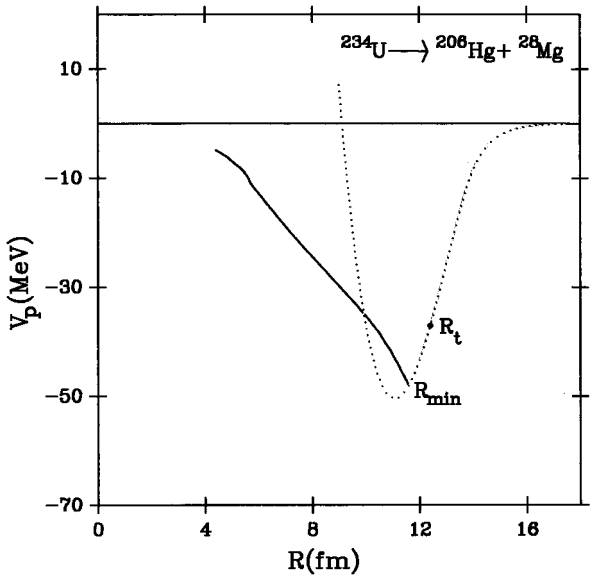

FIG. 2. The nuclear proximity potential between the deformed and pole-to-pole oriented decay products of $^{234}\mathrm{U}\rightarrow{}^{206}\mathrm{Hg}+{}^{28}\mathrm{Mg}$, allowing no neck (dotted line) and neck (solid line) formation. The touching configuration R_t and the new proximity minimum $R_{\min}$ due to neck effects are also labeled.

$$C^2=\epsilon^2, \tag{14a}$$

$$B^2=\frac{C^2(z_1^2+z_2^2)}{b_1^2+b_2^2-2C^2}. \tag{14b}$$

Substituting for B and C in (11), we get

$$V_P=\pi\gamma b^2\,\frac{(z_1^2+z_2^2)}{b_1^2+b_2^2-2\epsilon^2}\,\Phi_1(\xi=0). \tag{15}$$

For two equal nuclei, $z_1=z_2$, $b_1=b_2$ and we get the result of Molhotra and Gupta [11]. Note that Eq. (15) is valid as long as $2\epsilon^2<(b_1^2+b_2^2)$.

Figures 2 and 3 illustrate our calculated $V_P(R)$ for ^{28}Mg decays of ^{234}U and ^{238}Pu nuclei, respectively. In each figure, the dotted line represents the case of non-necked deformed and oriented nuclei [Eqs. (4) and (5) with s_0 and R given, respectively, by (8) and (10)] for the most probable pole-to-pole configuration [11] ($\theta_1=0°$ and $\theta_2=180°$) and deformation parameters β_{2i} taken from Ref. [21]. We notice that the shape of this potential is very much the same as for non-necked spherical nuclei (not plotted here). As already noted above, this potential is expected [10] to be less and less true as the overlap increases. Therefore, for the overlap region we have calculated the potential by using Eq. (15) for the necked configuration whose two center nuclear shape parameters (the two deformations β_{21}, β_{22} and neck parameter ϵ) are determined by minimizing the liquid drop energy expressed in these parameters [22]. This part of the potential for $R\leqslant R_{\min}$ is shown as a solid line. We notice that the potential now remains attractive and gives the correct asymptotic limit of going to zero at the parent nucleus radius, i.e., $V_P\rightarrow 0$ as the neck in Fig. 1(a) disappears and the relative separation $R(=z_1+z_2)\rightarrow 0$. Also, due to neck formation the minimum of the potential is shifted to a larger R value and that a part

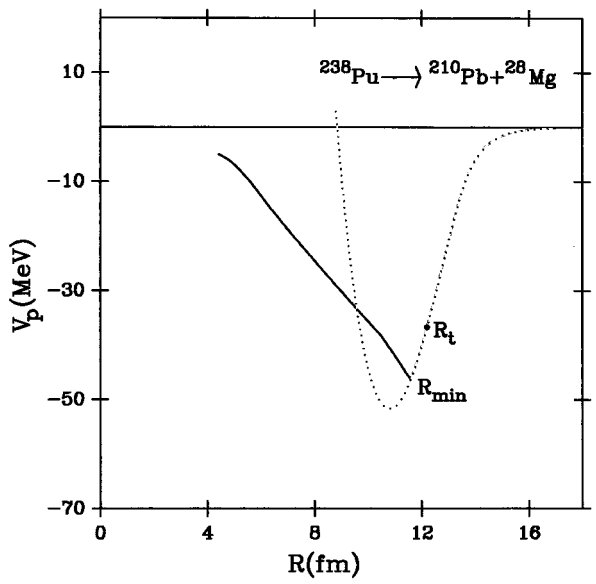

FIG. 3. Same as for Fig. 2 but for the decay $^{238}\mathrm{Pu}\rightarrow{}^{210}\mathrm{Pb}+{}^{28}\mathrm{Mg}$.

of the potential in the overlap region ($R_{\min}\leqslant R\leqslant R_t$) is still given by the pocket formula (4). Thus, the complete nuclear proximity potential for nuclei, with neck and deformation degrees of freedom included, is composed of two parts which are calculated separately, one for the necked configuration ($R\leqslant R_{\min}$) and other for non-necked deformed, oriented nuclei ($R\geqslant R_{\min}$). This is the nuclear proximity potential used in the following cluster decay calculations. Unfortunately, at present we do not know the way to go smoothly from a necked to non-necked configuration.

III. TOTAL INTERACTION POTENTIAL

The total interaction (or scattering) potential is given by

$$V(R)=E_C+V_P\,. \tag{16}$$

For spherical nuclei $E_C=Z_1Z_2e^2/R$, which for deformed and oriented nuclei is shown to be given by different expressions by different authors [23–26]. In the following we have used the one due to Wong [23], given for two nonoverlapping charge distributions as

$$E_C=\frac{Z_1Z_2e^2}{R}+\left(\frac{9}{20\pi}\right)^{1/2}\left(\frac{Z_1Z_2e^2}{R^3}\right)\sum_{i=1}^{2}R_{0i}^2\beta_{2i}P_2(\cos\alpha_i)$$
$$+\left(\frac{3}{7\pi}\right)\left(\frac{Z_1Z_2e^2}{R^3}\right)\sum_{i=1}^{2}R_{0i}^2[\beta_{2i}P_2(\cos\alpha_i)]^2. \tag{17}$$

The quadrupole-quadrupole interaction term proportional to $\beta_{21}\beta_{22}$ is neglected since it has a short-range character. Furthermore, in the absence of any useable prescription for calculating the Coulomb potential for two overlapping deformed nuclei, we have used Eq. (17) also for the overlap region. For spherical nuclei, the prescription of Kermode *et al.* [27] to calculate the Coulomb potential for necked configurations results in about the same result as for $E_C=Z_1Z_2e^2/R$.

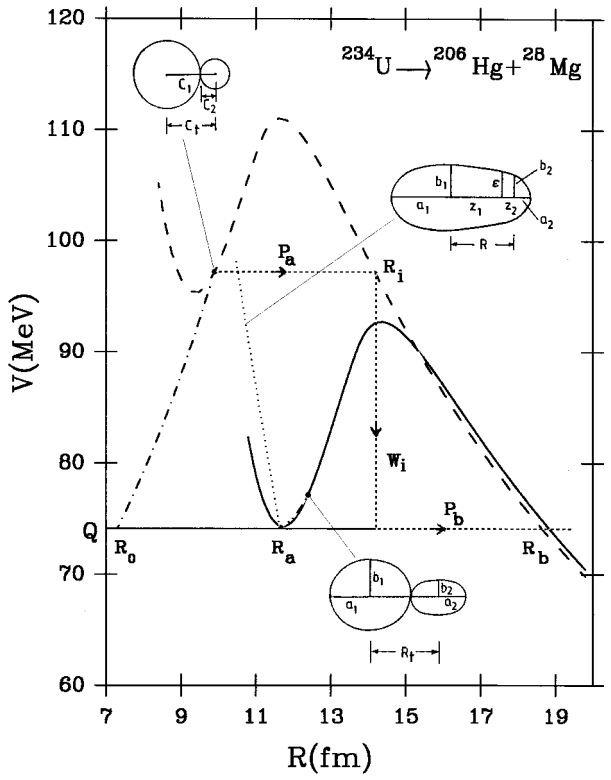

FIG. 4. The total interaction potential $V(R)=[V_P(R)+E_C(R)]$ for the decay products to be spheres (long-dashed line) or deformed and pole-to-pole oriented nuclei (solid line) in $^{234}\mathrm{U}\rightarrow{}^{206}\mathrm{Hg}+{}^{28}\mathrm{Mg}$. The dotted line represents the potential for the necked configuration in overlap region, meeting the Q value at $R=R_a$. The dot-dashed and dot-dot-dashed lines show the second-order polynomial interpolations, respectively, between the Q value at the parent nucleus radius R_0 and the touching configuration C_t for spherical nuclei and the Q value at the new proximity minimum R_a due to neck formation and the touching configuration R_t for deformed, oriented nuclei. The two center nuclear shape for the overlap region and the touching configurations for both the spherical and deformed nuclei are illustrated, along with the penetration paths for both the cases of spherical and deformed nuclei, respectively, as short-dashed lines and a solid line.

Figures 4 and 5 illustrate the total interaction potentials $V(R)$ for the ^{28}Mg decay of ^{234}U and the ^{32}Si decay of ^{238}Pu. The long-dashed lines represent the calculations for both the cluster and daughter nuclei to be spheres. The minimum due to proximity potential is also shown (marked $R_{\min}^{\mathrm{sph}}$ in Fig. 5). As in other cluster decay calculations [2–5], the potential at $R=C_t$ is extrapolated to Q value at $R=R_0$ via a second-order polynomial [see the dot-dashed line, referring to Eq. (19) below for $R_a\leqslant R\leqslant R_t$ with $R_a=R_0$ here].

The solid lines in Figs. 4 and 5 are the results of the calculations for non-necked (for both E_C and V_P) deformed and (pole-to-pole) oriented nuclei and the dotted lines are for the case where (two center) necked shapes are formed (for V_P only). [The potential energy minimum for the case of non-necked deformed, oriented nuclei is marked as $R_{\min}$ (see Fig. 5).] The necked configurations are considered up to a point where $V(R)=Q$ value. This value of R is denoted as R_a. Notice that R_a and $R_{\min}$ do not match exactly, perhaps due to the fact that the Coulomb potential E_C used here is

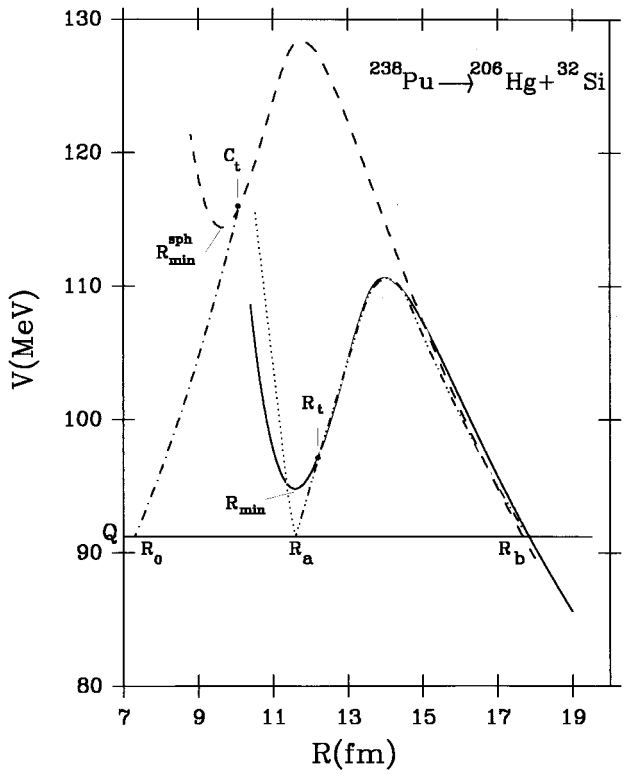

FIG. 5. Same as for Fig. 4 but for ^{238}Pu→^{206}Hg+^{32}Si. The potential energy minimum in both the cases of spherical ($R^{\rm sph}_{\rm min}$) and deformed ($R_{\rm min}$) nuclei are marked and the fit to the calculated potential for deformed and oriented nuclei (solid line for $R \geqslant R_t$) to the parametrized equation (19) is also shown (dot-dot-dashed line).

still for non-necked configurations (this is more so for ^{32}Si decay of ^{238}Pu in Fig. 5). Thus, the potential between R_a and R_t is again intrapolared via a second-order polynomial, along with the fit of the calculated potential (solid line) to Eq. (19) below for the analytical evaluation of the WKB penetrability P in Eq. (20) (the dot-dot-dashed line; the total fit is illustrated in Fig. 5 only). It is hoped that for the neck effects included in the Coulomb potential and the deformation effects averaged over all orientations, the above-mentioned intrapolated potential would represent the realistic proximity potential for the overlap region $R_a \leqslant R \leqslant R_t$.

We notice in Figs. 4 and 5 that due to deformations and orientations of nuclei the barrier is lowered as well as narrowed down considerably. Furthermore, it is moved to a larger R value and that the inner part of the interaction potential is determined to a good extent. Thus, for $V(R_a)=Q$ value, $R_a(\approx R_{\rm min}) > R_0$, in agreement with other models [6,7,9] using Dirac-δ, M3Y, and CW interactions. We shall see in the following sections that for exotic cluster decay studies these effects of deformations, orientations, and neck formation of nuclei are assimilated by choosing R_a in the neighborhood of R_t (or C_t), the touching configuration for spherical nuclei. In other words, the deformations, orientations, and neck formations of nuclei neglected in the earlier PCM calculations [1,8,12–18] of Gupta and collaborators are shown to get compensated by their choice of $R_a \approx R_t$ (or C_t) for both cluster preformation and WKB penetration probability. In cluster decay calculations, R_a refers to inner turning point of the WKB penetrability integral.

IV. THE PREFORMED CLUSTER MODEL

The cluster decay constant in a preformed cluster model (PCM) is given by Eq. (1). In the PCM of Malik and Gupta [8], the (spherical) cluster and daughter nuclei are considered to be preformed at $R \approx C_t$ with the quantum mechanical probability P_0 given by the solution of the stationary Schrödinger equation in mass asymmetry coordinate $\eta=(A_1-A_2)/(A_1+A_2)$. This theoretically calculated probability P_0 agrees completely with the empirical estimates of Blendowske and Walliser [28] for cluster masses $A_2 \leqslant 28$ and suggests a slight increase of P_0 for $A_2 > 28$ which then becomes nearly constant for $A_2 > 34$ (see, e.g., Fig. 13 in Ref. [1]; there are no other estimates known for $A_2 > 28$). The estimates of Blendowske and Walliser [28] are also based on theoretical calculations [9], made for some light clusters ($A_2 \leqslant 16$), and extrapolated empirically up to $A_2=28$. In view of this early success of PCM of Malik and Gupta (where both cluster and daughter nuclei were taken as spheres), in the following calculations (extended for deformations and neck formation effects), instead of calculating P_0 theoretically, we estimate $P_0^{\rm emp}(=\lambda_{\rm expt}/\nu_0 P)$ and compare them with the earlier empirically estimated P_0 of Blendowske and Walliser [28] and our own theoretically calculated P_0 mentioned above.

The tunnelling probability P in the model of Malik and Gupta [8] is the WKB penetrability, calculated analytically for the interaction potential $V(R)$ parametrized suitably [Eq. (19), illustrated in Fig. 5 as dot-dot-dashed line for the case of $V(R)$ calculated for non-necked deformed and oriented nuclei (the solid line)]. In earlier calculations [1,8,12–18] for both nuclei taken to be spheres, Gupta and collaborators choose the first (inner) turning point R_a at the touching configuration, i.e., $R_a=C_t$ (or R_t) and the second (outer) turning point R_b to give the Q value of the reaction, i.e., $V(R_b)=Q$ [see Fig. 4, the short-dashed line for spherical nuclei giving the tunneling path C_t to R_i with penetrability P_a, the internal deexcitation probability $W_i(=1)$ and then from R_i to R_b with penetrability P_b]. Later on, this restriction of choosing $R_a=R_t$ (or C_t) was relaxed [20,29] by letting R_a to be determined empirically ($R_a=R_{\rm emp}$) for a reasonable fit to the measured exotic-cluster decay half-lives. We obtained $R_{\rm emp}=R_t-\Delta R \approx R^{\rm sph}_{\rm min}$, the position of the minimum in the proximity potential for spherical nuclei. The value of $\Delta R = 0.7 \pm 0.15$ for many α and heavy cluster decays studied [29]. In the following, however, for deformed nuclei we choose R_a itself as the inner turning point, where $V(R_a)=Q$ value, and determine the WKB penetrability, given by

$$P = \exp\left(-\frac{2}{\hbar} \int_{R_a}^{R_b} [2\mu\{V(R)-Q\}]^{1/2} dR \right). \qquad (18)$$

Here, $\mu=mA_1A_2/(A_1+A_2)$ is the reduced mass with m as the nucleon mass. Note that for spherical nuclei (long-dashed lines) if we take $R_a=R_0$, Eq. (18) gives the result of Shi and Swiatecki [4] which predict very large $P_0^{\rm emp}$ (see Table I, case I for $\beta_{21}=\beta_{22}=0.0$).

For the potential $V(R)$ parametrized as

TABLE I. The penetrability P, assault frequency ν_0, product $\nu_0 P$, empirical preformation probability $P_0^{\rm emp}$, $-\log_{10} P_0^{\rm emp}$, and first turning point R_a (fm), calculated for some cluster decays using the preformed cluster model (PCM) of Malik and Gupta extended to include the deformations and neck formation effects. Other relevant quantities such as Q value, measured decay constant $\lambda_{\rm exp}(s^{-1})$ (taken from Ref. [1]) and deformations β_{21} and β_{22} of the daughter and cluster nuclei (taken from Ref. [21]) are also listed. Case I or II refers, respectively, to spherical or deformed, oriented nuclei. The orientations of the nuclei are fixed at $\theta_1=0°$, $\theta_2=180°$, referring to the so-called pole-to-pole configuration. Neck formation effects are included in case II.

Parent nucleus	Daughter nucleus	Emitted cluster	Q value (MeV)	$\lambda_{\rm exp}$ (s^{-1})	Case	β_{21} (Ref. [21])	β_{22} (Ref. [21])	R_a (fm)	P	ν_0 (s^{-1})	$\nu_0 P$ (s^{-1})	$P_0^{\rm emp}$ $\left(=\frac{\lambda_{\rm exp}}{\nu_0 P}\right)$	$-\log_{10} P_0^{\rm emp}$
^{224}Ra	^{220}Rn	^{4}He	5.79	2.19×10^{-6}	I	0.0	0.0	7.2	4.87×10^{-28}	2.89×10^{20}	1.40×10^{-7}	1.56×10^{1}	-1.19
					II	0.127	0.0	10.4	3.70×10^{-24}	2.89×10^{20}	1.07×10^{-3}	2.05×10^{-3}	2.69
	^{210}Pb	^{14}C	30.53	9.50×10^{-17}	I	0.0	0.0	7.2	4.27×10^{-38}	2.77×10^{20}	1.18×10^{-17}	8.03	-0.91
					II	0.023	0.361	10.2	3.04×10^{-27}	5.50×10^{20}	1.69×10^{-6}	5.62×10^{-11}	10.25
^{228}Th	^{208}Pb	^{20}O	44.72	7.48×10^{-22}	I	0.0	0.0	7.2	1.62×10^{-40}	2.55×10^{20}	4.13×10^{-20}	1.80×10^{-2}	1.74
					II	0.054	0.261	10.2	1.03×10^{-28}	4.33×10^{20}	4.46×10^{-8}	1.68×10^{-14}	13.78
^{234}U	^{210}Pb	^{24}Ne	58.84	5.94×10^{-26}	I	0.0	0.0	7.3	5.98×10^{-44}	2.77×10^{20}	1.66×10^{-23}	3.58×10^{-3}	2.45
					II	0.023	0.430	11.6	9.28×10^{-26}	4.08×10^{21}	3.79×10^{-4}	1.57×10^{-22}	21.80
	^{206}Hg	^{28}Mg	74.10	2.00×10^{-26}	I	0.0	0.0	7.3	1.60×10^{-42}	2.67×10^{20}	4.27×10^{-22}	4.68×10^{-5}	4.33
					II	0.069	0.485	11.7	4.29×10^{-20}	3.51×10^{20}	1.50×10^{1}	1.33×10^{-27}	26.89
^{238}Pu	^{210}Pb	^{28}Mg	75.93	1.38×10^{-26}	I	0.0	0.0	7.3	8.61×10^{-43}	2.68×10^{20}	2.31×10^{-22}	5.97×10^{-5}	4.22
					II	0.023	0.485	11.7	1.39×10^{-21}	6.89×10^{20}	9.58×10^{-1}	1.44×10^{-26}	25.84
	^{206}Hg	^{32}Si	91.21	3.47×10^{-26}	I	0.0	0.0	7.3	6.44×10^{-42}	2.55×10^{20}	1.64×10^{-21}	2.12×10^{-5}	4.67
					II	0.069	0.345	11.6	1.67×10^{-19}	5.75×10^{20}	9.58×10^{1}	3.62×10^{-28}	27.44
^{252}Cf	^{204}Pt	^{48}Ca	139.50	$<8.73\times10^{-17}$	I	0.0	0.0	7.5	2.73×10^{-39}	2.14×10^{20}	5.84×10^{-19}	$<1.50\times10^{2}$	<-2.17
					II	0.080	0.101	11.4	2.81×10^{-17}	5.43×10^{20}	1.53×10^{4}	$<5.69\times10^{-21}$	<20.24

$$V(R)=\begin{cases} Q+a_1R+a_2R^2, & R_a\leqslant R\leqslant R_t, \\ V(R_t)+m(R-R_t), & R_t\leqslant R\leqslant R_m, \\ V_B-\frac{1}{2}k(R-R_B)^2, & R_m\leqslant R\leqslant R_h, \\ V(R_h)-c\,\dfrac{R-R_h}{R}, & R_h\leqslant R\leqslant R_b, \end{cases} \tag{19}$$

the analytical solution of integral in Eq. (18) gives

$$\begin{aligned} P=\exp\Bigg(-\frac{2}{\hbar}\sqrt{2\mu}\Bigg\{ & \frac{\sqrt{a_2}}{2}\Bigg[t_1(t_1^2-L^2)^{1/2}-t_2(t_2^2-L^2)^{1/2} \\ & -L^2\Bigg(\cosh^{-1}\Big(\frac{t_1}{L}\Big)-\cosh^{-1}\Big(\frac{t_2}{L}\Big)\Bigg)\Bigg] \\ & +\frac{2}{3}\Bigg(\frac{R_m-R_t}{V(R_m)-V(R_t)}\Bigg)\{[V(R_m)-V(R_b)]^{3/2}-[V(R_t) \\ & -V(R_b)]^{3/2}\}-\frac{1}{\sqrt{2k}}[V_B-V(R_b)][\theta_2-\tfrac{1}{2}\sin 2\theta_2-\theta_1 \\ & +\tfrac{1}{2}\sin 2\theta_1]+\sqrt{cR_hR_b}[\theta_3-\tfrac{1}{2}\sin 2\theta_3]\Bigg\}\Bigg), \end{aligned} \tag{20}$$

with

$$a_1=\frac{R_a[Q-V(R_t)]}{R_t(R_t-R_a)},\quad a_2=-\frac{a_1}{R_a},$$

$$t_1=R_t-\tfrac{1}{2}R_a,\quad t_2=\tfrac{1}{2}R_a,$$

$$L^2=\tfrac{1}{4}R_a^2+R_t(R_t-R_a)\Big(\frac{Q-V(R_b)}{Q-V(R_t)}\Big),$$

$$\theta_1=\cos^{-1}\frac{R_m-R_B}{\sqrt{\alpha}_2},\quad \theta_2=\cos^{-1}\frac{R_h-R_B}{\sqrt{\alpha}_2},$$

$$\theta_3=\tan^{-1}\Big(\frac{R_b-R_h}{R_h}\Big)^{1/2},\quad \alpha_2=\frac{2}{k}[V_B-V(R_b)],$$

$$k=\frac{2\{[V_B-V(R_m)]^{1/2}+[V_B-V(R_h)]^{1/2}\}^2}{(R_m-R_h)^2},$$

$$c=\frac{R_b[V(R_h)-V(R_b)]}{R_b-R_h}.$$

Equation (19) means that the first part of the potential from R_a to R_t is a polynomial of degree two in R, the second part from R_t to R_m is a straight line of slope m, the top part between R_m and R_h is an inverted harmonic oscillator and the rest from R_h to R_b is a Coulomb potential of the type $1/R$. The V_B and R_B give the height and position of the barrier.

Finally, the assault frequency ν_0 is calculated in the harmonic oscillator approximation of the potential around $R=R_a$,

$$V(R)=Q+\tfrac{1}{2}K(R-R_a)^2. \tag{21}$$

which gives

$$\nu_0=\frac{1}{2\pi}\sqrt{\frac{K}{mA}}. \tag{22}$$

In earlier calculations [8,12–18] based on this model, ν_0 was defined in terms of the kinetic energy of the emitted cluster, obtained as its share of the Q value [$\nu_0=\sqrt{(2Q/mA_2)}/R_0$; mA_2 is the mass of the emitted cluster]. However, the order of ν_0 is the same for both calculations.

V. CALCULATIONS

The calculated penetrabilities P, the assault frequencies ν_0, the product ν_0P (called Gamow factor λ_G in the literature [1]) and the empirical preformation factors $P_0^{\rm emp}(=\lambda_{\rm exp}/\nu_0P)$, along with other characteristic quantities, for various exotic cluster decays are given in Table I for both the cases, I and II, of spherical and deformed, oriented nuclei, respectively. Also, the neck formation effects are included for case II of deformed nuclei. We notice that with the inclusion of neck and deformation effects of both the nuclei, the penetrability P increases and hence the preformation factor $P_0^{\rm emp}$ decreases considerably. The increase in P occurs due to the lowering and narrowing down of the barrier by the inclusion of neck and deformation effects (refer to solid line in Figs. 4 or 5).

Table I shows the results of α decay calculated for the ^{224}Ra parent. We notice that, for the case of deformation and neck effects included, our $P_0^{\rm emp}(\alpha)(=2.05\times10^{-3})$ is very close to the empirical estimate [$P_0(\alpha)=6.3\times10^{-3}$] of Blendowske and Walliser [28] for all parents. In view of this result, in the following we have normalized our $P_0^{\rm emp}(c)$ to $P_0(\alpha)$ of Blendowske and Walliser [28] and plotted the logarithms of this ratio in Fig. 6 as a function of cluster mass A_2. For comparisons, we have also plotted in this figure the empirical results of Blendowske and Walliser [28] [marked BW; given by the expression $P_0(c)/P_0(\alpha)=(6.3\times10^{-3})^{(A_2-4)/3}$ for even mass $A_2\leqslant28$] and another calculation due to Săndulescu *et al.* [7] (marked SGGCH) containing the deformation effects of only the emitted cluster(s). The following results are evident: (i) Our calculated $P_0^{\rm emp}(c)/P_0(\alpha)$ for $A_2\leqslant20$ match exactly with that of Blendowske and Walliser [28]. As already reminded before, the microscopic calculations [9], on which Blendowske and Walliser [28] based their empirical formula, were limited to lighter clusters ($A_2\leqslant16$) only. (ii) Beyond $A_2=20$, the straight line prescription of Blendowske and Walliser [28] does not seem to hold true, but the calculations of Săndulescu *et al.* [7], which include the deformation effects of only the clusters, are much closer to the present calculations which have the neck formation and deformation effects included for both the cluster and daughter nuclei. For $A_2\leqslant32$, the best straight line representation of our calculations is given by

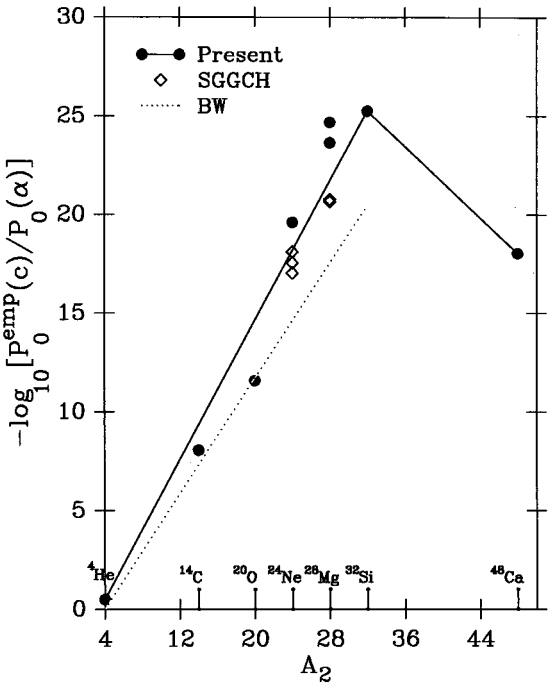

FIG. 6. The logarithms of the empirical cluster preformation probabilities relative to the α-particle preformation factor $[P_0(\alpha)=6.3\times10^{-3}]$ taken from Blendowske and Walliser [28] plotted as a function of mass number A_2 of the emitted cluster for the PCM of Malik and Gupta extended to include both the deformations and neck formations (filled circles and solid lines), compared with the empirical estimates of Blendowske and Walliser [28] (dashed line, marked BW) and the calculations of Săndulescu *et al.* [7] (open diamonds, marked SGGCH). The solid lines gives only the average behavior of the present calculations.

$$-\log_{10} P_0^{\rm emp}(c)=2.69+0.8839(A_2-4). \qquad (23)$$

(iii) $P_0^{\rm emp}$ decreases up to cluster mass $A_2=32$ and then starts to increase, which agrees with our earlier results [1,14] (e.g., compare the solid line in Fig. 6 with the solid line in Fig. 13 of Ref. [1]). Thus, comparing our present calculations with the earlier calculations of Gupta and collaborators [1,8,12–18] for spherical nuclei, it seems that the neck formation and deformation effects of the cluster and daughter nuclei included in the present calculations get compensated in the earlier calculations by their choosing the cluster preformation and first turning point (of WKB penetration integral) at the touching configuration of spherical nuclei which is close to inner (proximity) minimum of interaction potential ($R_a=C_t$ or $\approx R_{\rm min}^{\rm sph}$), rather than at the Q value.

Finally, a simplified model calculation is also carried out [19] by determining P_0 at R_a in the liquid drop model of Royer and collaborators [30], with shell effects included from Myers and Swiatecki [31]. For ^{28}Mg decay of ^{234}U, both taken to be deformed, we obtain $P_0=1.82\times10^{-5}$ and $T_{1/2}=1.6\times10^{20}$ s. Apparently, P_0 here compares rather well with the $P_0^{\rm emp}$ estimated above ($=4.7\times10^{-5}$ from Table I) at the same R_a but $T_{1/2}$ is off from the experimental value ($=3.46\times10^{25}$ s) by some orders of magnitude. This means that the calculated barrier, with deformations of nuclei included in the model of Royer and collaborators, is underes-timated for this case. Further calculations and their details will be published elsewhere.

VI. SUMMARY OF RESULTS

Based on the nuclear proximity approach [10,11], the interaction potential between any two deformed and pole-to-pole oriented nuclei forming a necked configuration in the overlap region is estimated. An asymmetric two center nuclear shape parametrization is used for the necked configuration. It is shown that due to deformations and orientations of nuclei, both the barrier height and width are reduced considerably. Also, the barrier position is shifted to a much larger R value and the energy minimum due to proximity is shifted down in the very neighborhood of the Q value with its R value, the $R_{\rm min}$, much larger than the radius R_0 of the compound nucleus. The role of the neck is shown to modify the nuclear potential around the proximity minimum ($R_{\rm min}$) by a small amount, as well as in obtaining the asymptotic limit of the nuclear proximity potential $[V_P(R_0)\rightarrow0]$ correctly. Since the neck formation effects on Coulomb potential between spherical nuclei are found to be negligible, the same between deformed nuclei are expected to be small and put the potential energy minimum exactly at the Q value.

For exotic cluster decay studies, the preformed cluster model of Malik and Gupta [8] is extended to include the above-mentioned deformation effects of both the emitted cluster and the daughter nucleus. Also, neck formation is allowed for the overlap region. These effects are shown to reduce the calculated empirical preformation probability considerably and in agreement with other earlier estimates based on shell model [28] and the M3Y potential with deformation effects of the cluster alone included in it [7]. Apparently, this result speaks of the success of our model for the cluster decay half-lives since the above noted earlier model calculations [7,28] are known to give good comparisons between their calculated $T_{1/2}$ values and the experimental data. In order to illustrate this result, an explicit model calculation for the decay half-life is also given.

Furthermore, the variation of our estimated $P_0^{\rm emp}(c)/P_0(\alpha)$ with cluster mass A_2 here matches with the earlier theoretical estimates of Gupta and collaborators [1,8,12–18] using the same model as here but for spherical nuclei. The preformation factor as well as first (inner) turning point are taken at the touching configuration of spherical cluster and daughter nuclei. This result suggests that the effects of neck formation and deformations of cluster and daughter nuclei in the present calculations get compensated in the earlier calculations of using spherical nuclei by starting the decay process (both cluster preformation and the penetrability) at the touching configuration of the spherical cluster and daughter nuclei. This is an important result for practical applications of the PCM of Malik and Gupta since, as already stated in the Introduction, the estimation of the deformations of all the possible fragmentations of a parent nucleus (for calculating the cluster preformation probability) are a rather tedious job.

[1] R. K. Gupta and W. Greiner, Int. J. Mod. Phys. (Suppl.) E **3**, 335 (1994).
[2] D. N. Poenaru, M. Ivascu, A. Sǎndulescu, and W. Greiner, Phys. Rev. C **32**, 572 (1985).
[3] G. A. Pik-Pichak, Sov. J. Nucl. Phys. **44**, 923 (1986).
[4] Y.-J. Shi and W. J. Swiatecki, Phys. Rev. Lett. **54**, 300 (1985).
[5] G. Shanmugam and B. Kamalaharan, Phys. Rev. C **38**, 1377 (1988).
[6] B. Buck and A. C. Merchant, Phys. Rev. C **39**, 2097 (1989).
[7] A. Sǎndulescu, R. K. Gupta, W. Greiner, F. Cǎrstoiu, and M. Horoi, Int. J. Mod. Phys. E **1**, 379 (1992).
[8] S. S. Malik and R. K. Gupta, Phys. Rev. C **39**, 1992 (1989); R. K. Gupta, in *Proceedings of the Fifth International Conference on Nuclear Reaction Mechanisms*, Varenna, Italy, 1988, edited by E. Gadioli (Ricera Scientifica Educazione Permanente, Italy), p. 416.
[9] R. Blendowske, T. Fliessbach, and H. Walliser, Nucl. Phys. **A464**, 75 (1987).
[10] J. Blocki, J. Randrup, W. J. Swiatecki, and C. F. Tsang, Ann. Phys. (N.Y.) **105**, 427 (1977).
[11] N. Malhotra and R. K. Gupta, Phys. Rev. C **31**, 1179 (1985).
[12] R. K. Gupta, W. Scheid, and W. Greiner, J. Phys. G **17**, 1731 (1991).
[13] S. Singh, R. K. Gupta, W. Scheid, and W. Greiner, J. Phys. G **18**, 1243 (1992).
[14] R. K. Gupta, S. Singh, R. K. Puri, A. Sǎndulescu, W. Greiner, and W. Scheid, J. Phys. G **18**, 1533 (1992).
[15] R. K. Gupta, S. Singh, R. K. Puri, and W. Scheid, Phys. Rev. C **47**, 561 (1993).
[16] R. K. Gupta, S. Singh, G. Münzenberg, and W. Scheid, Phys. Rev. C **51**, 2623 (1995).
[17] S. S. Malik, S. Singh, R. K. Puri, S. Kumar, and R. K. Gupta, Pramana **32**, 419 (1989); R. K. Puri, S. S. Malik, and R. K. Gupta, Europhys. Lett. **9**, 767 (1989).
[18] S. Kumar, D. Bir, and R. K. Gupta, Phys. Rev. C **51**, 1762 (1995); S. Kumar and R. K. Gupta, Phys. Rev. C **49**, 1922 (1994).
[19] R. K. Gupta and G. Royer (unpublished).
[20] R. K. Gupta, in *Frontier Topics in Nuclear Physics*, Proceedings of NATO Advanced Study Institute, Predeal, Romania, 1993, edited by W. Scheid and A. Sǎndulescu (Plenum, New York, 1994), pp. 129–140.
[21] S. Raman, C. H. Marlarkey, W. T. Milner, C. W. Nestor Jr., and P. H. Stelson, At. Data Nucl. Data Tables **36**, 1 (1987).
[22] H. J. Fink, W. Greiner, R. K. Gupta, S. Liran, H. J. Maruhn, W. Scheid, and O. Zohni, in *Proceedings of the International Conference on Reactions Between Complex Nuclei*, Nashville, Tennessee, 1974, edited by R. L. Robinson *et al.* (North Holland, Amsterdam, 1975), Vol. 2, p. 21; R. K. Gupta, Sov. J. Part. Nucl. **8**, 289 (1977); Nucl. Phys. Solid State Phys. (India) A **21**, 171 (1978); J. A. Maruhn, W. Greiner, and W. Scheid, *Heavy Ion Collisions*, edited by R. Bock (North Holland, Amsterdam, 1980), Vol. II, Chap. 6; R. K. Gupta, D. R. Saroha, and N. Malhotra, J. Phys. (Paris) Colloq. **45**, C6-477 (1984).
[23] C. Y. Wong, Phys. Rev. Lett. **31**, 766 (1973).
[24] R. Aroumougame and R. K. Gupta, J. Phys. G **6**, L155 (1980).
[25] M. Münchow, D. Hahn, and W. Scheid, Nucl. Phys. **A388**, 381 (1982).
[26] M. J. Rhoades-Brown, V. E. Oberacker, M. Seiwert, and W. Greiner, Z. Phys. A **310**, 287 (1983).
[27] M. W. Kermode, M. M. Mustafa, and N. Rowley, J. Phys. G **16**, L299 (1990).
[28] R. Blendowske and H. Walliser, Phys. Rev. Lett. **61**, 1930 (1988).
[29] S. Kumar, Ph.D. thesis, Panjab University, Chandigarh, 1992, India (unpublished).
[30] G. Royer and B. Remaud, Nucl. Phys. **A444**, 477 (1985); G. Royer and C. Piller, J. Phys. G **18**, 1805 (1992).
[31] W. D. Myers and W. J. Swiatecki, Nucl. Phys. **A601**, 141 (1996).